A tale of two shrimps – Speciation and demography of two sympatric shrimp species from hydrothermal vents

Author & Affiliations

Pierre Methou[1], Shannon B. Johnson[2], John Sherrin[3,4], Timothy M. Shank[5], Chong Chen[6], Verena Tunnicliffe[3,7]

[1]Univ Brest, Ifremer, CNRS, Unité Biologie des Environnements Extrêmes marins Profonds, Plouzané, France

[2]Monterey Bay Aquarium Research Institute (MBARI), Moss Landing, California, USA

[3]School of Earth & Ocean Sciences, University of Victoria, Victoria, British Columbia, Canada

[4]WSP Canada, Victoria, British Columbia, Canada

[5]Biology Department, Woods Hole Oceanographic Institution, 266 Woods Hole Rd., Woods Hole MA 02543, USA

[6]X-STAR, Japan Agency for Marine-Earth Science and Technology (JAMSTEC), Yokosuka, Kanagawa 237-0061, Japan

[7]Department of Biology, University of Victoria, Victoria, British Columbia, Canada

Abstract

Hydrothermal vents can serve as natural laboratories to study speciation processes due to their fragmented distribution often with geographic barriers between habitats. Two sympatric species of *Rimicaris* shrimps occur at vents on the Izu-Bonin-Mariana volcanic arc: *Rimicaris loihi* also occurs near Hawai'i and *R. cambonae* is present on the Tonga Arc. These two species biogeographically co-occur and are genetically similar, raising questions about their speciation mechanism, how they maintain distinct species, and whether interbreeding occurs. Here, we use barcoding and shotgun sequencing to test their genetic isolation and investigate their speciation process. We also evaluate population demography over 10 years to assess population densities and sex ratios at vents. Our results support *R. cambonae* and *R. loihi* as two distinct species despite sympatry throughout part of their range. We also observed regional-scale genetic structure among *R. loihi* populations from the Izu-Bonin-Mariana volcanic arc despite their broad geographic distribution. Finally, we found concomitant variations of shrimp densities and genetic diversity following fluctuations in geological and venting activities over a decade. A combination of geological instability,

ocean currents dynamics and sea-level changes might drive temporary isolation among these local populations. We suggest similar factors, with longer isolation periods, may also have promoted speciation between the two *Rimicaris* species whereas distinct life-history traits could strengthen and maintain reproductive barriers. Overall, our results indicate different connectivity patterns on a volcanic arc that contrast with those observed previously at vents from mid-ocean ridges or back-arc basins systems.

1. Introduction

Hydrothermal vent habitats on ocean ridges and volcanic arcs share characteristics with open ocean island archipelagos: they predominantly host endemic species, are isolated by expanses of inhospitable seafloor, and vulnerable to shifts in local conditions and the arrival of colonizing species. The dynamics of speciation on ocean island systems distal from mainland effects have been substantially explored in theoretical ecology (MacArthur & Wilson, 2001; Whittaker et al., 2008) amplified by studies on temporal processes and on regional phenomena such as volcanism or sea-level fluctuations (Fernández-Palacios, 2016). Much less is known about marine island-like settings. Seamount chains rising from the abyss, sometimes to sunlit depths, are possible analogies as the depth differences between them acting as dispersal barriers. Compared to the surrounding ocean floor, the upper slopes and crests of seamounts are often diversity hotspots (Morato et al., 2010). For the most part, seamount species are broadly distributed regionally although populations of some species show relatively poor connectivity; endemics are rare (Rogers, 2018). Marine organisms tend to have higher dispersal capabilities compared to their terrestrial counterparts, due to swimming adults or pelagic larval stages. Consequently, new subsea “islands” accumulate new species mostly by migration. Poor dispersers can speciate in isolated localities when gene flow diminishes, but radiation is deterred by new colonizers that may out-compete or interbreed with the incipient species (Pinheiro et al., 2017).

Hot vent ‘archipelagos’ along oceanic ridges, volcanic arcs, and back arc basins are notable for their high endemism (Tunnicliffe et al., 1998). Within a vent field, the steep thermal and chemical gradients generated by the mixing of vent fluids with seawater create a variable mosaic of distinct habitats constraining the spatial distribution of faunal communities (Cuvelier et al., 2011; Podowski et al., 2010). Even after45 years of both vent site and species discovery, rates of reported endemism have not diminished (Beaulieu & Szafrański, 2020; Tunnicliffe et al., 2023). Across eleven vent systems (= “archipelagos”) of the western Pacific, two-thirds of the species occur in only one system despite, in some cases, their close proximity; frequently, species in the same genus occupy identical

niches (Tunnicliffe et al., 2023). While connectivity studies at vents focus on taxa with broad ranges along mid-ocean ridges or back-arc basins, we know little about the speciation dynamics of poor dispersers or the outcomes of secondary contact by long-distance dispersers (Breusing et al., 2020; Castel et al., 2022; Johnson et al., 2013; Matabos & Jollivet, 2019; Thomas-Bulle et al., 2022). Connectivity of species living only at vents on volcanic arcs have also received less attention. Overall, the biogeographic histories and responses of marine organisms living in underwater "islands" may differ significantly from terrestrial counterparts living on islands. Case studies from hot vents, as key examples of underwater archipelagos, provide the basis for comparative assessments.

Among the vent-endemic fauna, species of *Rimicaris* shrimps are commonly found living in sympatry in several regions, where two or three species can co-occur within the same vent fields (Lunina & Vereshchaka, 2014; Methou, Hernández-Ávila, et al., 2022; Methou, Chen, et al., 2024). In most cases, *Rimicaris* shrimps exhibit broad geographic distributions with high genetic connectivity along mid-ocean ridges (Beedessee et al., 2013; Teixeira et al., 2012; Zhou et al., 2022) or back-arc basins (Methou, Ogawa, et al., 2024; Thaler et al., 2014; Yahagi et al., 2015), suggesting a high dispersal potential. As with most decapods, *Rimicaris* shrimps are gonochoric brooders that maintain their eggs under their abdomen but also display a variety of reproductive cycles with seasonal or aperiodic brooding patterns (Copley & Young, 2006; Methou, Chen, et al., 2022; Methou et al., 2023). In some *Rimicaris* species, brooding cycles were unrelated to variations in photosynthetic surface production, unlike other seasonal brooders that inhabit vents (Methou, Chen, et al., 2022).

Two sympatric *Rimicaris* species co-occur at vents from the Izu-Bonin-Mariana (IBM) Volcanic Arc in the Northwest Pacific: *Rimicaris* (formerly *Opaepele*) *loihi* and the recently described *R. cambonae* (Methou, Chen, et al., 2024). The hydrothermally-active habitats of *R. loihi* and *R. cambonae* are highly diverse and volatile, characterized by areas of liquid CO_2 emergence at NW Eifuku, molten sulfur ponds at Nikko Seamount and other sites with an extensive record of historical eruptive events (Embley et al., 2007; Lupton et al., 2006). In particular, active eruptions occurred at NW Rota Volcano during each of the six visits between 2004 and 2010 (Chadwick et al., 2008, 2012; Embley et al., 2006; Schnur et al., 2017). *Rimicaris loihi* was also reported from distant sites including Loihi Seamount off the southeast coast of Hawai'i (Williams & Dobbs, 1995) and at West Mata Volcano north of Tonga (Resing et al., 2011). West Mata and Loihi are also unstable due to seismic and eruptive activities, as recorded at Loihi in 1996 and by *in situ* observations of explosive eruptions during dives at West Mata in 2008 and 2009 (Garcia et al., 2006; Resing et al., 2011).

The sympatric *R. cambonae* and *R. loihi* are also genetically similar, differing by just 2% in the barcoding region of the mitochondrial cytochrome *c* oxidase subunit I (*COI*) gene fragment (Methou, Chen, et al., 2024) and thus falling at the broad border between divergent populations and species

(Hebert et al., 2003). Given that they coexist within the same faunal assemblages, questions arise about the presence of gene flow and, thus, the effectiveness of reproductive barriers despite the potential for reproduction. However, data on the reproductive biology of these species are limited to one single population of *R. loihi* from Suiyo collected in August 2019, that revealed a largely female-biased sex ratio and presence of many juveniles and ovigerous females (Methou et al., 2023).

This study aims to answer the following questions: 1) Are nuclear genes of *R. loihi* and *R. cambonae* concordant with mitochondria and represent separate species-level lineages?; 2) Is there gene flow and hybridisation between *R. cambonae* and *R. loihi* or is there a complete reproductive isolation?; 3) To what extent does the eruptive and unstable geological context affect the population dynamics of these shrimps over the years?; and 4) What is the most likely scenario for their speciation?

2. Materials and Methods

2.1 Animal sampling and processing

Alvinocaridid shrimps were collected during eight oceanographic expeditions between 2004 and 2023 using suction samplers or baited traps on either Remotely Operated Vehicles (ROVs) or Human Operated Vehicles (HOVs). In total, five hydrothermal vent fields from the Izu-Bonin-Mariana (IBM) Volcanic Arc were visited once (Seamount X in 2006, Suiyo in 2019), twice (Nikko in 2006 and 2010, NW Eifuku in 2004 and 2023) or six times (NW Rota between 2004 and 2014) (Figure 1A). Additional shrimps were collected in 2004 at Loihi Seamount near Hawai'i, the type locality of *Rimicaris loihi* and in 2009 at the West Mata volcano (Figure 1A; see Table S1 for detailed sampling information).

Specimens were preserved either in 75% ethanol or frozen whole at -80°C on-board the ship. Additional specimens from NW Eifuku in 2023 were fixed with 4% paraformaldehyde (PFA) for 3h on board and stored in 50% phosphate-buffered saline (PBS)-ethanol solution for electron microscopy (see Supplementary Methods). We determined sex based on examination of 1st and 2nd pleopod shape and measured the size of each shrimp as carapace length (CL) and/or total length (TL) following (Methou, Chen, et al., 2024). For the few ovigerous females encountered, we estimated realized fecundity from egg counts and sizes. For 144 specimens collected in 2023 at NW Eifuku, we distinguished *R. cambonae* and *R. loihi* based on morphological characters defined by (Methou, Chen, et al., 2024) – briefly, the form of the pterygostomial tooth on the front part of the carapace and the shape of the proximolateral tubercle on the antennular stylocerite – in conjunction with *COI*

130 barcoding. However, as specimens from earlier work were no longer available for morphological
131 study, species identification reported below relies on genetic assessment.

132 **2.2 Shrimp Abundance**

133 On NW Rota, vents occur in the upper 80 m of the summit. Fine-scale mapping with an
134 SM2000 system, good ROV navigation, and physical markers (e.g., Schnur et al. 2017) supported
135 comparative estimates of volcanic activity and venting extent between years. However, rugged
136 terrain and radical changes in the volcano topography hampered repeated transects. Instead, we
137 estimated shrimp abundance each year by assessing the total fraction of the ROV transects in which
138 shrimps were visible in densities greater than ~20 individuals/m^2.

139 **2.3 DNA extraction and Sanger sequencing**

140 We performed DNA extractions on 597 alvinocaridid shrimps using the 4th/5th pleopods or
141 pieces of abdominal tissues following manufacturer's instructions of the DNeasy Blood & Tissue kit
142 (Qiagen, Hilden, Germany). We amplified the 5' region of the cytochrome *c* oxidase subunit I gene
143 (*COI*) with the Cari-COI-1F and Cari-COI-1R alvinocaridid primers (Methou et al., 2020) for shrimps
144 collected from Nikko 2010, Suiyo 2019, and NW Eifuku 2023 (679 to 734 bp fragment) or with the
145 COI-1f (5'-AGTAGGAACAGCCCTTAGTCTCCTA-3') and COI-1r (5'-TCCCGCTGGGTCAAAGAATGAGG-3')
146 primers for the remaining shrimps (529 to 623 bp fragment).

147 We used Promega GoTaq polymerase in 25µl reactions for PCR amplifications with Cari-COI-
148 1F and Cari-COI-1R and iProof High Fidelity DNA Polymerase (Bio-Rad) in 40µl reactions for PCR
149 amplifications with COI-1f and COI-1r using 1 µl of the DNA template for both. We conducted PCR
150 with the following cycle conditions: initial denaturation at 95°C for 5 min, 35 cycles of 95°C (1 min),
151 50°C (1 min), 72°C (2 min), followed by a final extension stage of 72°C for 7 min with Cari-COI primers
152 or initial denaturation at 95°C for 5 min, 35 cycles of 95°C (1 min), 50°C (1 min), 72°C (2 min),
153 followed by a final extension stage of 72°C for 7 min with the COI-1f/ COI-1r primers.

154 Bi-directional Sanger sequencing was conducted by Eurofins (Köln, Germany) for PCR
155 products amplified with Cari-COI-1F/ Cari-COI-1R primers and by the High Throughput Genomics Unit
156 (Seattle, WA, USA) for PCR products amplified with COI-1f/COI-1r primers. We edited and aligned
157 sequence chromatograms with Geneious Prime® 2023.1.2 (https://www.geneious.com).

158 **2.4 Haplotype networks**

159 To assign individual mitochondrial barcodes to putative species, we used the Assemble-
160 Species-by-Automatic-Partitioning method on a 529-bp alignment, a method based on the detection
161 of "barcode gaps" (Puillandre et al., 2021). We estimated median joining haplotype networks with

162 PopART v1.7 (Bandelt et al., 1999; Leigh & Bryant, 2015) with default settings. We used DnaSP v6
163 (Rozas et al., 2017) to determine the number of variable sites (*S*), the number of haplotypes (*h*),
164 haplotype diversities (H_d), nucleotide diversities (π), average number of nucleotide differences (*k*,
165 (Tajima, 1983), raw genetic distance (D_a), and pairwise F_{ST} values with 1000 permutations within and
166 among putative species and populations.

167 **2.5 Whole Genome Shotgun Sequencing and Analyses**

168 **2.5.1 Sequencing**

169 Following *COI* barcoding, we used whole genome shotgun (WGS) sequencing on a subset of
170 randomly selected animals of each species along our sampling range on the IBM volcanic arc to
171 examine whether nuclear data were concordant with mitochondrial data and to explore connectivity
172 amongst populations and lineages. We quantified genomic DNA with the DNA High-Sensitivity assay
173 with the Qubit 2.0 Fluorometer (ThermoFisher Scientific, Waltham MA, USA) and prepared 32
174 individuals for WGS sequencing with the Illumina DNA Prep kit (Illumina, Inc. San Diego, CA). We
175 sequenced six randomly chosen individuals of *R. loihi* from Suiyo and Nikko, eight from Eifuku, and
176 four from NW Rota Seamounts. We also sequenced eight *R. cambonae* from Eifuku Seamount.
177 Sequences were generated on the Element Bio AVITI instrument at UC Davis with a paired-end 2x150
178 protocol. Low coverage individuals, including all four specimens from NW Rota were unsuccessful
179 and were excluded from analyses.

180 **2.5.2 Quality filtering**

181 We first removed sequencing barcodes and adapters from WGS data with Trimmomatic
182 v.0.35 (Bolger et al., 2014). To perform population genetic analyses on WGS sequencing, we filtered
183 mitochondrial and PhiX sequencing control data from nuclear reads with the programs BWA MEM
184 v.0.7.17, seqtk, and SAMTools v1.7-1. We then assembled a nuclear genome from the individual that
185 had the highest number of reads (OC_Ebi50, *R. cambonae* from Eifuku Seamount) with SPAdes
186 (v.3.15.5-Linux, (Prjibelski et al., 2020) with default settings. We examined the assembly with the
187 program BandageNG v.2022.8-dev (https://github.com/asl/BandageNG) and removed contigs <1500
188 bp long.

189 We mapped reads from genomic data to the nuclear genome that we assembled for the
190 Ebi50 individual with the program ANGSD v0.940 (Korneliussen et al., 2014). Average read depth was
191 plotted against the sequencing read score quality for all individuals, which enabled us to visualize the
192 data and limit low quality reads, paralogs, and repetitive regions of the genome. Low-coverage
193 individuals, including one *R. loihi* and *R. cambonae* each from NW Eifuku and all four specimens from
194 NW Rota were excluded from analyses. We took a number of steps to filter our data within ANGSD to

195 only include high-quality reads. We discarded reads that had multiple hits to the reference assembly
196 (paralogs) and limited read depths from 10-150x coverage where we discarded reads <10x and
197 >150x coverage. We increased SNP site mapping quality by filtering excessive mismatches (C=50),
198 removed all sites with missing data, excluded improperly paired reads, and adjusted qscores around
199 indels to resolve false variants. Each population was individually tested for deviations from the
200 Hardy-Weinberg Equilibrium (HWE, p-value <0.05) and sites that were statistically significant were
201 excluded from subsequent analyses.

202 **2.5.3 Statistics and demographic analyses**

203 We used the programs ANGSD, PCAngsd (Meisner & Albrechtsen, 2018), ngsTools v3.0
204 (https://github.com/mfumagalli/ngsTools), ∂a∂i v. 2.3.7 (Gutenkunst et al., 2009), StAMPP
205 (Pembleton et al., 2013) and dadi-pipeline v.3.1.7 (Portik et al., 2017) to estimate population and
206 species differentiation, admixture, and demographic histories of populations. With ANGSD, we
207 estimated genotype likelihoods and the minor allele frequency (MAF) to calculate the site frequency
208 spectrum (SFS), to estimate population differentiation; (F_{ST}, Reynolds et al., 1983), and summary
209 statistics with at least five individuals per site. Lacking an ancestral sequence to polarize data, we
210 calculated Tajima's D, Waterson's Θ, and Nucleotide diversity (π) from the SFS with a 'folded'
211 spectrum where each SNP was present in at least five individuals and had a minimum minor allele
212 frequency of 0.05. We also used the R package StAMPP (v.1.6.3, (Pembleton et al., 2013) to calculate
213 F_{ST} values, 95% confidence limits, and *p*-values among populations and species. To do so we
214 estimated the SFS within ANGSD for the entire dataset with the same filtering parameters as above
215 for sites that at least ten individuals had data and with the -doSaf (1) flag which calculates the site
216 allele frequency likelihood based on individual genotype likelihoods assuming HWE, -doPost (1) flag
217 which uses the allele frequencies as a prior, the -doMaf (1) flag which calculates fixed major and
218 minor per-site frequencies, the -doMajorMinor (1) flag which infers major and minor allele
219 frequencies from the genotype likelihoods, the -doGeno flag (32) which writes the posterior
220 probabilities of the genotypes as binary with a snp_pvalue of $1e^{-6}$. We then used realSFS to estimate
221 the site frequency spectra, then imported these within a second run of ANGSD, with the same
222 parameters but also including the -doPest flag with the results from realSFS and the -doBcf flag
223 which exports a BCF file. We then used BCFtools (v.1.11-21-g0987715, (Danecek et al., 2021) to
224 convert the bcf file to a vcf file for import to R. Within R, we used vcfR (v.1.15.0, (Knaus & Grünwald,
225 2017) to import the VCF file for analyses in StAMPP.

226 We used the dadi_pipeline to infer the joint demographic histories of populations with the
227 folded joint allele frequency spectrum estimated from ANGSD and realSFS from each population SFS
228 estimate. To create an input file for ∂a∂i we formatted the outfile with the perl script: realsfs2dadi.pl

229 (https://github.com/z0on/2bRAD_denovo /blob/master/realsfs2dadi.pl). We tested the three-
230 population pipeline but analyses never concluded, so instead we used the dadi-pipeline two-
231 population script in a pairwise fashion where the spectra were folded (Charles et al., 2018; Portik et
232 al., 2017). First, we compared the sympatric populations of *R. loihi* and *R. cambonae* from Eifuku
233 seamount. Second, we compared the allopatric populations of *R. cambonae* from Eifuku and *R. loihi*
234 from Nikko seamount. We chose the Nikko population because it was geographically closest to the
235 Eifuku locality. Third, we compared each *R. loihi* population. We used the dadi-test-projections.py
236 script from the dadi_pipeline to determine the number of projections to maximize the number of
237 segregating sites. We tested both the 'diversification model set' (Portik et al., 2017) and 'island
238 model set' (Charles et al., 2018) for two populations. The diversification set tests models that range
239 from no migration to more complicated models that include secondary contact and population size
240 changes. We also included the island model diversification set since hydrothermal vents are often
241 compared to isolated island habitats. Dadi_pipeline analyses were run with the default settings from
242 10-40 replicates for four optimization rounds each, where at the end of each round, the parameters
243 of the best-scoring replicate are used to generate the starting parameters of the next round. Once
244 completed, the lowest AIC value was compared with the Summarize_outputs.py script to find the
245 model that best-fit our data. We plotted results with the Make_plots.py script.

246 We estimated principal component analysis and population admixture of individual
247 genotypes probabilities with ANGSD with the same filtering parameters as above but also removed
248 sites that were not in HWE. Within ANGSD, we used a MAF of 0.05 and sites where at least 5
249 individuals had SNP data with a p-value of 10^{-3} to estimate a covariance matrix for PCA for PCAngsd
250 and NGSadmix v.32 (Skotte et al., 2013). We ran NGSadmix five times for each population (K) value
251 and then used the method of Evanno et al. (2005) to compute the most probable number of clusters
252 for NGSadmix analyses, however, we also looked at patterns of clustering from our data since the
253 method often underestimates K (Gilbert et al., 2012; Janes et al., 2017; Waples & Gaggiotti, 2006).
254 We used ANGSD to compute genetic distances from genotype probabilities and ngsDist (Vieira et al.,
255 2016) for a multiple dimensional scaling analysis (MDS) with the same parameters used for PCA.
256 Results were visualized in the tidyverse (Wickham et al., 2019) with RStudio (Posit team, 2025) and R
257 (R Core Team, 2021).

258 **2.6 Mitochondrial genomic phylogeny**

259 We extracted mitochondrial genomic data from WGS reads with the programs BWA MEM
260 v.0.7.17, seqtk, and SAMTools v1.7-1 with the published mitochondrial genome (NC_020311) and
261 mapped them within the program Geneious Prime®2024.0.7. We also aligned genomes with the

MAFFT algorithm and tested mitochondrial genome alignments for the best phylogenetic model with Modeltest with AIC (Darriba et al., 2020) within Geneious Prime. We used the program MrBayes v3.2.7 (Ronquist et al., 2012) to estimate a phylogeny of mitochondrial genomes including published data from other members of the Alvinocaridae and other closely related deep-sea shrimp. We ran multiple analyses for 10 million generations, sampled every 1000 generations with six chains, and discarded the first 10% of trees as a burnin. We examined multiple runs to ensure we achieved convergence in Tracer v.1.7.2 (Rambaut et al., 2018). Consensus trees were visualized with TreeViewer v.2.2.0 (Bianchini & Sánchez-Baracaldo, 2023). The mitogenome map was visualized with the CG view server (Stothard & Wishart, 2004, http://cgview.ca).

3. Results

3.1 Distribution, densities, and habitat preference

The two identified species of *Rimicaris* had different distributions. We found *Rimicaris loihi* at five sites on the Izu-Bonin-Mariana (IBM) arc across 1900 km and on Loihi Volcano more than 6000 km to the east (Figure 1A). It was the only species of shrimp on Suiyo, Nikko, and Loihi volcanoes, although the sample size at Loihi was small (7 individuals); however, it is not recorded at seven other IBM vent sites. *Rimicaris loihi* was the dominant species on NW Rota where, of the 332 specimens confirmed via *COI* identification, only three were *R. cambonae* (0.9%). In contrast, *R. cambonae* was the dominant species in 2023 NW Eifuku collections at 90.3%. However, in the small 2004 sample from the same site, only two of the 25 specimens collected were *R. cambonae*. Finally, 12 *R. cambonae* were identified from the West Mata vent field in the Southwest Pacific as the only species present.

R. loihi appeared most abundant on sulphur crusts at all collection sites but were also observed on surfaces of andesitic lavas at NW Rota and among mussels at both NW Eifuku and Suiyo. At NW Eifuku in 2023, *R. cambonae* co-occurred with *R. loihi* within mussel beds and on bare rocks.

Repeated exploration of NW Rota vent field between 2004 and 2010 revealed that, as eruption intensity and venting varied over the years, so did the abundance of shrimps (Table 2, Figure 2B–E). For 2004, we estimated average shrimp densities around vents to be 386 m^{-2} (n=6; SD=165); maximum adult densities exceeded 900 m^{-2} in 2009 when shrimps were most abundant (Figure 2B). In the rugged terrain, it was not possible to map the distribution of shrimp species, however we observed that along the known sites, the abundance of shrimps mirrored the venting extent, peaking in 2009 at 45%. The lowest abundances of shrimps were in 2006 during intense

294 eruptions when shrimps were tightly clustered around a few vent openings, and in 2014, when
295 volcanic activity had ceased and hydrothermal venting contracted to the central eruption pit (Table 2;
296 Figure 2E).

297 **3.2 *COI* haplotype network and genetic diversity**

298 Our Assemble-Species-by-Automatic-Partition (ASAP) analysis to assess putative species
299 revealed two partitions that had equal support (lowest ASAP score of 2.50; Figure S1): individuals fell
300 into either two or three genetic groups. Our morphological identifications of 144 shrimps from NW
301 Eifuku corresponded to two groups; assigned to *Rimicaris loihi* and *R. cambonae*. The third *COI*
302 lineage identified in the three partitions result included distinct *R. cambonae* haplotypes from NW
303 Rota. Distribution of pairwise differences was bimodal with two distinct Gaussian distributions and
304 showed no overlap (Figure S1). F_{ST} values also supported genetic differentiation for two groups, and
305 possibly a third, with high values between *R. cambonae* and *R. loihi* and, to a smaller extent,
306 between *R. cambonae* from NW Eifuku and from NW Rota (Table S2). The partitions were evident
307 with a relatively low genetic distance (between *R. cambonae* from NW Eifuku and NW Rota (D_a =
308 0.009) compared to the higher genetic distance between *R. cambonae* and *R. loihi* (D_a = 0.023).

309 Species delineation was also clear based on the *COI* haplotype network; it comprised 158
310 haplotypes from 597 barcoded individuals, of which 134 were assigned to *R. loihi* and 24 to *R.*
311 *cambonae* (Figure 1D). *Rimicaris loihi* and *R. cambonae* showed distinct genetic characteristics with a
312 much lower haplotype diversity for *R. cambonae* compared to *R. loihi* (H_d = 0.499 ± 0.052 and H_d =
313 0.877 ± 0.011, respectively) and almost three-fold lower nucleotide diversity for *R. cambonae* (π =
314 0.00190 and π = 0.00437; Table S3). Similarly, the average number of nucleotide differences was
315 lower for *R. cambonae* (k= 1.048) than for *R. loihi* (k= 2.208), a trend that did not appear to be
316 related to sample size differences, with a similarly high value for *R. loihi* (k = 2.534) when randomly
317 subsampled to the same sample size as *R. cambonae*. The West Mata population of *R. cambonae* had
318 higher levels of haplotype diversity (H_d), nucleotide diversity (π), and average nucleotide differences
319 (k) compared to the northern *R. cambonae* populations from the IBM arc (Table S3); the southern
320 population also had two intermediate haplotypes, although they are closer to *R. cambonae* than *R.*
321 *loihi* (Figure 1D). Haplotype variability among populations of *R. loihi* was notably higher than the
322 sympatric *R. cambonae*, where Suiyo was the most diverse and Nikko was the least diverse (Table S3).

323 To explore further the possibility of temporal metapopulation dynamics of *R. loihi*, we
324 estimated a separate haplotype network and summary statistics for NW Rota data only (Figure 2F).
325 Yearly data were similar except for 2006 and 2014 when there was slightly lower nucleotide diversity
326 (π), as well as lower average nucleotide differences (k) (Table S4).

327 **3.3 Mitochondrial genome phylogeny**

328 We aligned 26 mitochondrial genomes from *R. cambonae* and *R. loihi* recovered from WGS
329 data. Mitochondrial genomic alignments showed the same pattern of divergence between the two
330 species as the *COI* fragment and differed by 1.5% for the GTR substitution model. The mitochondrial
331 genome of each species had the same gene composition and arrangement as all other published
332 mitochondrial genomes of the Alvinocarididae (Figure 3).

333 **3.4 Whole Genome Shotgun sequencing**

334 Our Whole Genome Shotgun (WGS) sequencing of *Rimicaris* individuals resulted in 109
335 million reads that included 19 *R. loihi* from NW Eifuku, Suiyo, and Nikko seamounts and seven *R.*
336 *cambonae* from NW Eifuku (Figure 4A) after we excluded low-coverage individuals. The assembled
337 reference genome from our most successfully sequenced individual of *R. cambonae* from NW Eifuku
338 (Ebi50) recovered a relatively poor assembly of ~62.8 m bases with an average coverage of 6x. After
339 we removed scaffolds <1500 bp long the remaining assembly included 1332 scaffolds of 6 million
340 base pairs with an average coverage of 13x and a N50 of 2790 bp.

341 **<u>3.4.1 Population Statistics</u>**

342 We estimated summary statistics within each population to examine whether they were in
343 equilibrium (Figure S2). Estimates of summary statistics for *R. loihi* included 2,175,571 sites from
344 Suiyo, 2,539,205 sites from Nikko, 2,641,049 sites from Eifuku, and 2,837,793 sites from *R. cambonae*
345 from Eifuku seamounts. The mean Tajima's D statistic for all populations was similar and slightly
346 positive, although the values were higher for both species from NW Eifuku (T_{cam} = 1.0, T_{loh} = 1.1) than
347 *R. loihi* from Nikko (T_{lohN} = 0.6) or Suiyo (T_{lohS} = 0.6) they were still below the threshold indicative of
348 balancing selection or strong population contraction. The mean per-site nucleotide diversity ranged
349 from 0.01–0.02 and was lowest in the *R. cambonae* from NW Eifuku population and highest for the *R.*
350 *loihi* population at Nikko seamount. Mean per-site estimates of Waterson's θ also were relatively low,
351 and ranged from 0.01–0.02 and again was lowest for *R. cambonae* from NW Eifuku and highest for *R.*
352 *loihi* from Nikko seamounts.

353 **<u>3.4.2 Species delineation</u>**

354 We first used genomic data to assess whether nuclear loci were concordant with
355 mitochondrial data and whether they supported *R. loihi* and *R. cambonae* as distinct species. After
356 quality filtering, our covariance matrix for PCA included 111,002 sites and revealed population
357 segregation where the majority of differentiation was between *R. loihi* and *R. cambonae* (Figure 4).
358 The MDS plot which was based on genetic distances included 126,652 sites and showed that, among
359 *R. loihi* populations, the one from NW Eifuku was the most closely related to *R. cambonae* from the

360 same site.

361 Genotypic admixture plots were estimated with 111,002 sites for two to five populations also
362 revealed differentiation between *R. cambonae* and *R. loihi* (Figure S3). The Evanno method showed
363 the most probable number of admixture clusters was four, however the ΔK for two populations was
364 undefined due to a low likelihood variance between K=2 and K=3.

365 F_{ST} estimates between the species were relatively low, however we detected some
366 subdivision. Global weighted F_{ST} estimates calculated within ANGSD between the populations ranged
367 from 0.103–0.175, where they were lowest between *R. cambonae* and Suiyo seamount *R. loihi* and
368 highest between *R. cambonae* and Nikko Seamount *R. loihi* (Table S5). F_{ST} estimates calculated with
369 StAMPP were similar to those from ANGSD/realSFS, where they were again low, but all population
370 comparisons were significant (Table S6).

371 When we compared the demographic histories and possible migration between sympatric
372 populations of *R. cambonae* and *R. loihi* from NW Eifuku with the dadi-pipeline we included 141,021
373 segregating sites with projection sizes of 14 alleles for each species (Figure 5, Table S7). We did not
374 rescale our estimates because we did not have an appropriate mutation rate. We found the most
375 probable model that fit our data was no migration between the species (no_mig, AIC=153626, Figure
376 S4). The next most probable models were divergence with continuous asymmetrical migration
377 (asym_mig, AIC=155126), divergence with different migration rates, with instantaneous population
378 size changes (asym_mig_size, AIC=157445), and divergence with no gene flow, followed by
379 instantaneous size changes with continuous asymmetrical migration (sec_contact_asym_mig_size,
380 AIC=157458, table S7). When we compared allopatric populations of *R. cambonae* from NW Eifuku
381 and *R. loihi* from Nikko seamount we included projections sizes of 14 and 12 alleles for each
382 population respectively for 138,269 segregating sites. The most probable model between the
383 allopatric populations was for a split with no migration, then instantaneous size change with no
384 migration (no_mig_size, AIC=144207, Table S8). The next most probable models were divergence
385 with no gene flow, followed by instantaneous size changes with continuous asymmetrical migration
386 (sec_contact_asym_mig_size, AIC=145792), no migration (no_mig, AIC=147041), and divergence
387 with continuous asymmetric migration (anc_asym_mig, AIC=147130, Table S8).

388 **3.4.3 Gene Flow within *R. loihi***

389 We also found some subdivision among *R. loihi* populations with MDS and PCA analyses
390 (Figure 4). The NW Eifuku population was the most distinct from Nikko or Suiyo populations, a result
391 reflected by higher F_{ST} values (0.013–0.075, Table S5 and S6). Despite the relative geographic
392 proximity of Nikko and NW Eifuku, there is low probability of larval exchange between them due to
393 ocean current direction (Figure 1, Mitarai et al., 2016). We found low amounts differentiation

394 between Nikko and Suiyo seamounts. The most probable admixture plots for three or more
395 populations also showed that *R. loihi* from NW Eifuku appeared somewhat divergent and the Suiyo
396 population was a mixture of Nikko and NW Eifuku genotypes (Figures 4 and S3).

397 Pairwise estimates of demographic histories and migration among three populations of *R.*
398 *loihi* from Suiyo, Nikko and NW Eifuku seamounts from dadi_pipeline analyses also remained
399 unscaled because we lacked an appropriate mutation rate. Pairwise analyses based on a folded
400 spectrum between *R. loihi* populations confirmed patterns of subdivision. We included 136,936
401 segregating sites with projections for 12 alleles from both Suiyo and Nikko seamounts. We found the
402 most probable model for Suiyo-Nikko interaction was a split with continuous symmetrical migration
403 followed by instantaneous size change (anc_sym_mig_size, AIC=130546, Figure 6, Table S9). The
404 three next most probable models were only slightly less so but involved patterns of admixture
405 instead of migration (Table S9). When we compared 157,151 segregating sites for 12 and 14 allele
406 projections for Nikko and NW Eifuku, we found the most probable model was an island model:
407 vicariance, middle unidirectional discrete admixture event between two drift events
408 (vic_two_epoch_admix, AIC=181429). The next most probable models either involved no migration
409 or a split with continuous symmetric migration, followed by isolation. Lastly, when we compared
410 128,388 segregating sites for 12 and 14 allele projections the most probable model for comparisons
411 between Suiyo and NW Eifuku also had no migration but was a founder event with a middle
412 unidirectional discrete admixture event (between two drift events)
413 (founder_nomig_admix_two_epoch, AIC=129489). However, two of the three next most probable
414 models both had asymmetric migration from Suiyo into NW Eifuku populations (Table S9).

415 **3.4 Population sex ratio and reproductive traits**

416 The sex ratio of *R. loihi* from NW Rota was significantly female skewed for each year (χ^2 =
417 25.64 – 259.69, $p < 0.001$; Table 1), as previously observed in the Suiyo population (Methou et al.,
418 2023). A similar trend occurs for the sex ratio of *R. loihi* from NW Eifuku, but was not statistically
419 supported ($\chi^2 = 1.33$, $p > 0.05$) probably due to a low sample size (Table 1). Conversely, the sex ratio
420 of *R. cambonae* from NW Eifuku did not significantly deviate from 1:1 ($\chi^2 = 1.09$, $p > 0.05$; Table 1).
421 Despite large sampling sizes, ovigerous females of *R. loihi* were nearly absent from populations
422 collected at NW Rota in March (2004 and 2009) and April (2006 and 2010) with only two ovigerous
423 females out of 408 females in these years (Figure 4A). Similarly, no ovigerous females were collected
424 among the 72 females of *R. cambonae* from NW Eifuku in March 2023 (Figure 6A). However, four
425 ovigerous females out of 380 females were collected at NW Rota in December 2014 (Figure 6A) and
426 larger numbers were observed peripheral to venting (but not sampled; Figure 6B). With 110 to 387
427 eggs per brood (11.4 to 44.4 eggs mm^{-1}), relative fecundities of *R. loihi* ovigerous females from NW

428 Rota were in the range reported at Suiyo with 61 to 356 eggs per brood (10.2 to 49.2 eggs mm^{-1}),
429 (Figure 6C) (Methou et al., 2023).

430

431 ## 4. Discussion

432 Nuclear genomic data confirmed previous results based on the mitochondrial *COI* fragment and
433 morphology suggesting that *Rimicaris loihi* and *Rimicaris cambonae* constitute two separate species
434 (Methou, Chen, et al., 2024). This segregation into two distinct species was further supported by our
435 demographic modelling analyses that indicated strict isolation with no migration as the most
436 probable model; thus, gene flow has likely stopped between *R. cambonae* and *R. loihi* despite their
437 sympatric distribution.

438 Genetic structure is also present among the different populations of *R. loihi* along the Izu-Bonin-
439 Mariana (IBM) arc. Yet, demographic histories supported ancient migration or secondary contact as
440 the most probable model, suggesting that some level of gene flow is maintained between
441 populations from Suiyo to NW Eifuku. Patterns of genetic structure for *R. loihi* populations was not
442 simply a result of distance since we observed a greater genetic similarity between the more
443 geographically distant populations of Suiyo and Nikko than with NW Eifuku, which is closer to Nikko.
444 This pattern contrasts with most vent endemic species in the West Pacific that exhibit high genetic
445 homogeneity within-basin or within-arc structures (Breusing et al., 2021; Poitrimol et al., 2022; Tran
446 Lu Y et al., 2022, 2025). Only the copepod *Stygiopontius lauensis,* whose geographic distribution is
447 constrained within the Lau Basin, shows similar patterns of structured populations at a regional scale
448 (Diaz-Recio Lorenzo et al., 2024). However, such structuration at a small spatial scale on the IBM arc
449 was unexpected for *R. loihi*, especially given its broad distribution outside the region, including to
450 Loihi Seamount near Hawaii. This broad geographic distribution also applies to its sister species,
451 since previous reports of *R. loihi* at West Mata volcano (Resing et al., 2011) actually represent *R.*
452 *cambonae* according to our barcoding analyses.

453 Alvinocaridid shrimps are generally considered as good dispersers with high genetic connectivity
454 over long distances as observed in many species (Methou, Ogawa, et al., 2024; Thaler et al., 2014;
455 Yahagi et al., 2015; Zhou et al., 2022). For example, *R. exoculata* lacks genetic structure over 7100 km,
456 likely supported by Mid-Atlantic Ridge ocean circulation promoting connectivity (Teixeira et al., 2012).
457 Morphological features of their hatched larvae including *R. loihi* also supports a long pelagic larval
458 duration (PLD) (Hernández-Ávila et al., 2015; Methou et al., 2023). However, calculated probabilities
459 for larval exchange among our sites are low (Mitarai et al. 2016). The dominant upper ocean
460 currents in this region are across, not along, the Arc in an east to west direction (Kendall & Poti,

2014), thus most larvae are advected away from the Arc although some may be retained.

The genetic structuration among regional *R. loihi* populations is likely also driven the particular geological context of the IBM arc and enforced by ocean currents. Several hydrothermal vent fields on the IBM volcanic arc are characterized by high geological instability (Embley et al., 2007; Lupton et al., 2006). At NW Rota, our observations over 10 years revealed repeated eruptions with significant variation in the extent of venting activities. Shrimp abundance over the years reflected these changes of venting that also affected their genetic diversity as the NW Rota population declined or expanded. This strong instability of habitat availability may lead to repeated local contraction/extinction of *R. loihi* at some sites on a temporary basis; rupture of connecting nodes could isolate shrimp populations to less connected areas, such as the northern or southern parts of the IBM arc (Mitarai et al., 2016). This limited connectivity at a regional scale may explain the absence of *R. loihi* at several IBM vent sites (Brunner et al., 2022) and the apparent lack of *R. cambonae* (or cf. *loihi*) beyond the northern Tonga-Tofua volcanos of the SW Pacific. These shrimps also appear to have specific habitat requirements linked to the volcanic emissions or sulphur substratum that characterize all the sites colonized by both species.

Sea level changes during glaciation periods may also have contributed to the temporary isolation of *R. loihi* populations. During the Last Glacial Maximum, sea-level decrease could have transformed shallowest arc volcanoes into subaerial volcanoes, eliminating chemosynthetic habitats that could serve as potential stepping stones for vent endemic species like *Rimicaris* shrimps. This contrasts with what we know from terrestrial archipelagos where sea level drop may have reduced isolation between some islands (Fernández-Palacios, 2016; Weigelt et al., 2016). Periods of relative quiescence in volcanism and venting associated with episodic delivery of magma in the rising melt (Stern et al., 2003) may also have prevented the establishment of chemosynthetic fauna during these intervals.

The same mechanisms that drive geological instability at a local scale or related to ocean currents and sea-level changes may also have promoted speciation between *R. cambonae* and *R. loihi* by isolating two ancestral populations for a sufficient period of time. The genetic similarity between *R. cambonae* and *R. loihi* is closest on NW Eifuku; initial separation may have occurred at this site or between ancestral population not in our analyses. This could include populations from the southern part of the Mariana arc (i.e., NW Rota) or from the more remote populations of West Mata in the Tonga arc or Loihi seamount near Hawaii. Given the predominant eastward North Pacific Drift, the latter site is mostly likely a sink, not a source, location. Larval dispersal among volcanic arc systems or back-arc basins in the West Pacific is inferred to be infrequent and directional, following oceanic currents (Mitarai et al., 2016; Tunnicliffe et al., 2023). In particular, transit is deemed highly

495 improbable between south and north hemispheres as larvae transport is inhibited by the strong
496 Equatorial Counter Current and Equatorial Undercurrent that both flow eastward in the upper 300 m
497 with little water movement below (Constantin & Johnson, 2015). Thus, relatively few hydrothermal
498 vent species distributions cross the equator (Tunnicliffe et al., 2023). A rare circumstance of long-
499 distance dispersal from either the IBM southward or the Tonga-Tofua Arc northward could have
500 established an outpost population in the distal arc; we cannot determine the direction. Subsequent
501 geological instability in both volcanically active regions may have affected shrimp population sizes
502 and genetic diversities to different extents in both source and recipient sites. The current sympatric
503 distribution of both *R. loihi* and *R. cambonae* in the Mariana Arc likely results from secondary contact
504 by another rare larval dispersal event from south to north. This scenario of speciation by allopatry
505 postulates that genetic inflow via larval dispersal between the two regions was disrupted for a
506 sufficiently long period to generate an isolation phase that would persist and be maintained in
507 sympatry.

508 Genetic isolation between sympatric sister species could be maintained by strong reproductive
509 barriers. Differences in reproductive mode (egg laying versus brooding) strengthens reproductive
510 isolation between the syntopic sister species of intertidal snails *Littorina saxatilis* and *L. arcana*
511 (Stankowski et al., 2020). In coastal isopods of the *Jaera* species complex, sexual isolation between
512 co-occurring species is reinforced by preferential mate choice even with some level of hybridization
513 and no influx from parental populations (Ribardière et al., 2017, 2021). Allochronic isolation with
514 different reproductive seasonality can also maintain genetic differentiation as reported in
515 Mediterranean pine moths (Santos et al., 2007). However, our dataset on the reproductive
516 characteristics of *R. loihi* and *R. cambonae* remains inconclusive on the possible existence of such
517 barriers to reproduction. As with most carideans (Correa & Thiel, 2003), alvinocaridid shrimps are all
518 gonochoric species that mate and brood their eggs under their abdomen until larval release (Methou,
519 Chen, et al., 2022; Methou et al., 2023). A wide variety of reproductive cycles occur in this family,
520 including aperiodic or periodic brooding patterns, with or without synchronicity to seasonal
521 variations (Copley & Young, 2006; Methou, Chen, et al., 2022; Methou et al., 2023). The presence of
522 numerous ovigerous individuals of *R. loihi* both in August and December – despite a notable and
523 repeated absence in March/April – does not point to a periodicity distinct from its sister species. We
524 did find that populations of *R. loihi* from the Mariana Arc, as at Suiyo (Methou et al., 2023), were
525 largely biased toward females whereas the proportion of males and females was roughly equal for *R.*
526 *cambonae*. This discrepancy between the sex ratios of the two species could indicate different
527 mating choice, as variation in adult sex ratios can strongly influence breeding systems and mate
528 choice in many animal groups (Grant & Grant, 2019; Székely et al., 2014). Yet assortative mating

between the two *Rimicaris* species remains to be demonstrated. Further studies using larger genomic dataset across the entire range of the two species as well as investigations on their trophic and reproductive ecology will be required to clarify mechanisms leading to their speciation.

5. Conclusion

Rimicaris loihi and *R. cambonae* are two distinct, recently diverged species living in sympatry throughout a part of their geographic range. Hybridisation does not appear to occur between the two species. Analysing genetic data from shrimps collected from a single vent over a decade revealed variability in genetic diversity that correlates with local eruption events, suggesting that population dynamics of these shrimps are impacted by their unstable habitats. Although our demographic analyses remain inconclusive as to how speciation occurred among these two species, we propose allopatric divergence and a secondary contact by a long-distance dispersal event as the most likely scenario. The geographic overlap and recent divergence of this species pair makes them an interesting case study for a future exploration into speciation mechanisms that may provide insights to how species arise in insular habitats overall. Our findings also have an important implication on conservation, showing widespread distribution does not equate to resilience. Local disturbances such as volcanic eruptions or anthropogenic impacts like deep-sea mining might not cause these species to go extinct but can exterminate genetically distinct populations, with limited potential for recovery via recolonization.

Acknowledgments

We thank Dr. Craig Moyer for providing shrimp specimens from Loihi Seamount. We also thank Joe Jones and Lara Puetz for their work on genetic barcoding for some specimens. Captain and crew of R/Vs *Yokosuka*, *Kaimei,* and *Natsushima* are gratefully acknowledged for their continued support of our scientific activities during the cruises YK19-10, KM23-E05, and NT10-13 Leg 2, respectively. We extend this to the pilots and technical teams of HOVs *Shinkai 6500* and *Pisces V*, as well as ROVs *Hyper-Dolphin, KM-ROV, Jason-2,* and *ROPOS*. This is a GACHINKO Cruise Episode I (19-10) output, and we thank the GACHI-participants for their help in sorting shrimp specimens on-board. We thank the cruise chief scientists Ken Takai (JAMSTEC; YK19-10, KM23-E05) and Shinji Tsuchida (JAMSTEC; NT10-13 Leg 2), as well as Shinsuke Kawagucci (JAMSTEC) whose successful cruise proposal led to the sampling on the Mariana volcanic arc during cruise KM23-E05. Sampling during cruise KM23-E05 within the Islands Unit of the Mariana Trench Marine National Monument of the United States of America was carried out under the special use permit SUP 12542-23001 (MSR U2022-047). We are grateful for collections during several cruises in the NOAA Ring of Fire series of the Vents Program on

the Mariana Volcanic Arc. Chief Scientists Bob Embley, Bill Chadwick, and Dave Butterfield were critical to the output.

Funding

PM was supported by ISblue project, Interdisciplinary graduate school for the blue planet (ANR-17-EURE-0015) and co-funded by a grant from the French government under the program "Investissements d'Avenir" embedded in France 2030. PM also benefited from French State aid managed by the National Research Agency under France 2030: ANR-22-POCE-0007. VT was supported by NSERC Canada and the Canada Research Chairs programme. Whole Genome Shotgun Sequencing was funded by the David and Lucile Packard Foundation at MBARI.

References

Bandelt, H.-J., Forster, P., & Röhl, A. (1999). Median-joining networks for inferring intraspecific phylogenies. *Molecular Biology and Evolution*, *16*(1), 37–48. https://doi.org/10.7882/FS.2004.039

Beaulieu, S. E., & Szafrański, K. M. (2020). *InterRidge Global Database of Active Submarine Hydrothermal Vent Fields Version 3.4* [Dataset]. PANGAEA. https://doi.org/10.1594/PANGAEA.917894

Beedessee, G., Watanabe, H., Ogura, T., Nemoto, S., Yahagi, T., Nakagawa, S., Nakamura, K., Takai, K., Koonjul, M., & Marie, D. E. P. (2013). High Connectivity of Animal Populations in Deep-Sea Hydrothermal Vent Fields in the Central Indian Ridge Relevant to Its Geological Setting. *PLoS ONE*, *8*(12), e81570. https://doi.org/10.1371/journal.pone.0081570

Bianchini, G., & Sánchez-Baracaldo, P. (2023). TreeViewer: Flexible, modular software to visualise and manipulate phylogenetic trees. *Ecology and Evolution*, *14*(2), 1–16. https://doi.org/10.1002/ece3.10873

Bolger, A. M., Lohse, M., & Usadel, B. (2014). Trimmomatic: A flexible trimmer for Illumina sequence data. *Bioinformatics*, *30*(15), 2114–2120. https://doi.org/10.1093/bioinformatics/btu170

Breusing, C., Johnson, S. B., Mitarai, S., Beinart, R. A., & Tunnicliffe, V. (2021). Differential patterns of connectivity in Western Pacific hydrothermal vent metapopulations: A comparison of

biophysical and genetic models. *Evolutionary Applications*, *August*, 1–14. https://doi.org/10.1111/eva.13326

Breusing, C., Johnson, S. B., Tunnicliffe, V., Clague, D. A., Vrijenhoek, R. C., & Beinart, R. A. (2020). Allopatric and sympatric drivers of speciation in alviniconcha hydrothermal vent snails. *Molecular Biology and Evolution*, *37*(12), 3469–3484. https://doi.org/10.1093/molbev/msaa177

Brunner, O., Chen, C., Giguère, T., Kawagucci, S., Tunnicliffe, V., Kayama, H., & Satoshi, W. (2022). Species assemblage networks identify regional connectivity pathways among hydrothermal vents in the Northwest Pacific. *Ecology and Evolution*, *October*, 1–15. https://doi.org/10.1002/ece3.9612

Castel, J., Hourdez, S., Pradillon, F., Daguin-Thiébaut, C., Ballenghien, M., Ruault, S., Corre, E., Tran Lu Y, A., Mary, J., Gagnaire, P.-A., Bonhomme, F., Breusing, C., Broquet, T., & Jollivet, D. (2022). Inter-Specific Genetic Exchange Despite Strong Divergence in Deep-Sea Hydrothermal Vent Gastropods of the Genus Alviniconcha. *Genes*, *13*(6), 985. https://doi.org/10.3390/genes13060985

Chadwick, W. W., Cashman, K. V., Embley, R. W., Matsumoto, H., Dziak, R. P., De Ronde, C. E. J., Lau, T. K., Deardorff, N. D., & Merle, S. G. (2008). Direct video and hydrophone observations of submarine explosive eruptions at NW Rota-1 volcano, Mariana arc. *Journal of Geophysical Research: Solid Earth*, *113*(B8), 2007JB005215. https://doi.org/10.1029/2007JB005215

Chadwick, W. W., Dziak, R. P., Haxel, J. H., Embley, R. W., & Matsumoto, H. (2012). Submarine landslide triggered by volcanic eruption recorded by in situ hydrophone. *Geology*, *40*(1), 51–54. https://doi.org/10.1130/G32495.1

Charles, K. L., Bell, R. C., Blackburn, D. C., Burger, M., Fujita, M. K., Gvoždík, V., Jongsma, G. F. M., Kouete, M. T., Leaché, A. D., & Portik, D. M. (2018). Sky, sea, and forest islands: Diversification in the African leaf-folding frog *Afrixalus paradorsalis* (Anura: Hyperoliidae) of the Lower Guineo-Congolian rain forest. *Journal of Biogeography*, *45*(8), 1781–1794.

https://doi.org/10.1111/jbi.13365

Constantin, A., & Johnson, R. S. (2015). The dynamics of waves interacting with the Equatorial Undercurrent. *Geophysical & Astrophysical Fluid Dynamics*, *109*(4), 311–358. https://doi.org/10.1080/03091929.2015.1066785

Copley, J. T. P., & Young, C. M. (2006). Seasonality and zonation in the reproductive biology and population structure of the shrimp Alvinocaris stactophila (Caridea: Alvinocarididae) at a Louisiana Slope cold seep. *Marine Ecology Progress Series*, *315*(June), 199–209. https://doi.org/10.3354/meps315199

Correa, C., & Thiel, M. (2003). Mating systems in caridean shrimp (Decapoda: Caridea) and their evolutionary consequences for sexual dimorphism and reproductive biology. *Revista Chilena de Historia Natural*, *76*(2), 187–203. https://doi.org/10.4067/S0716-078X2003000200006

Cuvelier, D., Pierre-Marie Sarradin, Sarrazin, J., Colaço, A., Copley, J. T., Desbruyeres, D., Glover, A. G., Santos, R. S., & Tyler, P. A. (2011). Hydrothermal faunal assemblages and habitat characterisation at the Eiffel Tower edifice (Lucky Strike , Mid-atlantic Ridge). *Marine Ecology*, *32*, 243–255. https://doi.org/10.1111/j.1439-0485.2010.00431.x

Danecek, P., Bonfield, J. K., Liddle, J., Marshall, J., Ohan, V., Pollard, M. O., Whitwham, A., Keane, T., McCarthy, S. A., Davies, R. M., & Li, H. (2021). Twelve years of SAMtools and BCFtools. *GigaScience*, *10*(2), giab008. https://doi.org/10.1093/gigascience/giab008

Darriba, D., Posada, D., Kozlov, A. M., Stamatakis, A., Morel, B., & Flouri, T. (2020). ModelTest-NG: A New and Scalable Tool for the Selection of DNA and Protein Evolutionary Models. *Molecular Biology and Evolution*, *37*(1), 291–294. https://doi.org/10.1093/molbev/msz189

Diaz-Recio Lorenzo, C., Tran Lu Y, A., Brunner, O., Arbizu, P. M., Jollivet, D., Laurent, S., & Gollner, S. (2024). Highly structured populations of copepods at risk to deep-sea mining: Integration of genomic data with demogenetic and biophysical modelling. *Molecular Ecology*, *33*(9), e17340. https://doi.org/10.1111/mec.17340

Embley, R., Baker, E., Butterfield, D., Chadwick, W., Lupton, J., Resing, J., De Ronde, C., Nakamura, K.,

Tunnicliffe, V., Dower, J., & Merle, S. (2007). Exploring the Submarine Ring of Fire: Mariana Arc - Western Pacific. *Oceanography*, *20*(4), 68–79. https://doi.org/10.5670/oceanog.2007.07

Embley, R., Chadwick, W. W., Baker, E. T., Butterfield, D. A., Resing, J. A., De Ronde, C. E. J., Tunnicliffe, V., Lupton, J. E., Juniper, S. K., Rubin, K. H., Stern, R. J., Lebon, G. T., Nakamura, K., Merle, S. G., Hein, J. R., Wiens, D. A., & Tamura, Y. (2006). Long-term eruptive activity at a submarine arc volcano. *Nature*, *441*(7092), 494–497. https://doi.org/10.1038/nature04762

Evanno, G., Regnaut, S., & Goudet, J. (2005). Detecting the number of clusters of individuals using the software STRUCTURE: A simulation study. *Molecular Ecology*, *14*(8), 2611–2620. https://doi.org/10.1111/j.1365-294X.2005.02553.x

Fernández-Palacios, J. M. (2016). Shaped by sea-level shifts. *Nature*, *532*(7597), 42–43. https://doi.org/10.1038/nature17880

Garcia, M. O., Caplan-Auerbach, J., De Carlo, E. H., Kurz, M. D., & Becker, N. (2006). Geology, geochemistry and earthquake history of L?ihi Seamount, Hawaìi's youngest volcano. *Geochemistry*, *66*(2), 81–108. https://doi.org/10.1016/j.chemer.2005.09.002

Gilbert, K. J., Andrew, R. L., Bock, D. G., Franklin, M. T., Kane, N. C., Moore, J.-S. B., Moyers, B. T., Renaut, S. B., Rennison, D. J., Veen, T., & Vines, T. H. (2012). Recommendations for utilizing and reporting population genetic analyses: The reproducibility of genetic clustering using the program structure. *Molecular Ecology*.

Grant, P. R., & Grant, B. R. (2019). Adult sex ratio influences mate choice in Darwin's finches. *Proceedings of the National Academy of Sciences of the United States of America*, *116*(25), 12373–12382. https://doi.org/10.1073/pnas.1903838116

Gutenkunst, R. N., Hernandez, R. D., Williamson, S. H., & Bustamante, C. D. (2009). Inferring the Joint Demographic History of Multiple Populations from Multidimensional SNP Frequency Data. *PLoS Genetics*, *5*(10), e1000695. https://doi.org/10.1371/journal.pgen.1000695

Hebert, P. D. N., Ratnasingham, S., & De Waard, J. R. (2003). Barcoding animal life: Cytochrome *c*

oxidase subunit 1 divergences among closely related species. *Proceedings of the Royal Society of London. Series B: Biological Sciences*, *270*(suppl_1). https://doi.org/10.1098/rsbl.2003.0025

Hernández-Ávila, I., Cambon-Bonavita, M. A., & Pradillon, F. (2015). Morphology of first zoeal stage of four genera of alvinocaridid shrimps from hydrothermal vents and cold seeps: Implications for ecology, larval biology and phylogeny. *PLoS ONE*, *10*(12), 1–27. https://doi.org/10.1371/journal.pone.0144657

Janes, J. K., Miller, J. M., Dupuis, J. R., Malenfant, R. M., Gorrell, J. C., Cullingham, C. I., & Andrew, R. L. (2017). The *K* = 2 conundrum. *Molecular Ecology*, *26*(14), 3594–3602. https://doi.org/10.1111/mec.14187

Johnson, S. B., Won, Y.-J., Harvey, J. B., & Vrijenhoek, R. C. (2013). A hybrid zone between Bathymodiolus mussel lineages from eastern Pacific hydrothermal vents. *BMC Evolutionary Biology*, *13*, 21. https://doi.org/10.1186/1471-2148-13-21

Kendall, M. S., & Poti, M. (2014). Potential larval sources, destinations, and self-seeding in the Mariana Archipelago documented using ocean drifters. *Journal of Oceanography*, *70*(6), 549–557. https://doi.org/10.1007/s10872-014-0251-7

Knaus, B. J., & Grünwald, N. J. (2017). VCFR: A package to manipulate and visualize variant call format data in R. *Molecular Ecology Resources*, *17*(1), 44–53. https://doi.org/10.1111/1755-0998.12549

Korneliussen, T. S., Albrechtsen, A., & Nielsen, R. (2014). ANGSD: Analysis of Next Generation Sequencing Data. *BMC Bioinformatics*, *15*(356). https://doi.org/10.1186/s12859-014-0356-4

Leigh, J. W., & Bryant, D. (2015). POPART: full-feature software for haplotype network construction. *Methods in Ecology and Evolution*, *6*, 1110–1116. https://doi.org/10.1111/2041-210X.12410

Lunina, A. A., & Vereshchaka, A. L. (2014). Distribution of hydrothermal alvinocaridid shrimps: Effect of geomorphology and specialization to extreme biotopes. *PLoS ONE*, *9*(3). https://doi.org/10.1371/journal.pone.0092802

Lupton, J., Butterfield, D., Lilley, M., Evans, L., Nakamura, K., Chadwick, W., Resing, J., Embley, R., Olson, E., Proskurowski, G., Baker, E., De Ronde, C., Roe, K., Greene, R., Lebon, G., & Young, C. (2006). Submarine venting of liquid carbon dioxide on a Mariana Arc volcano. *Geochemistry, Geophysics, Geosystems*, *7*(8), 2005GC001152. https://doi.org/10.1029/2005GC001152

MacArthur, R. H., & Wilson, E. O. (2001). *The theory of island biogeography* (Vol. 1). Princeton university press.

Matabos, M., & Jollivet, D. (2019). Revisiting the Lepetodrilus elevatus species complex (Vetigastropoda: Lepetodrilidae), using samples from the Galápagos and Guaymas hydrothermal vent systems. *Journal of Molluscan Studies*, *85*(1), 66–72. https://doi.org/10.1093/mollus/eyy061

Meisner, J., & Albrechtsen, A. (2018). Inferring Population Structure and Admixture Proportions in Low-Depth NGS Data. *Genetics*, *210*(2), 719–731. https://doi.org/10.1534/genetics.118.301336

Methou, P., Chen, C., Kayama, Watanabe, H., Cambon, M.-A., & Pradillon, F. (2022). Reproduction in deep-sea vent shrimps is influenced by diet, with rhythms apparently unlinked to surface production. *Ecology and Evolution*, *June*, 1–12. https://doi.org/10.1002/ece3.9076

Methou, P., Chen, C., & Komai, T. (2024). Revision of the alvinocaridid shrimp genus Rimicaris Williams & Rona, 1986 (Decapoda: Caridea) with description of a new species from the Mariana Arc hydrothermal vents. *Zootaxa*, *5406*(4), 501–518. https://doi.org/10.11646/zootaxa.5406.4.1

Methou, P., Hernández-Ávila, I., Cathalot, C., Cambon-Bonavita, M.-A., & Pradillon, F. (2022). Population structure and environmental niches of Rimicaris shrimps from the Mid-Atlantic Ridge. *Marine Ecology Progress Series*, *684*, 1–20. https://doi.org/10.3354/meps13986

Methou, P., Michel, L. N., Segonzac, M., Cambon-Bonavita, M.-A., & Pradillon, F. (2020). Integrative taxonomy revisits the ontogeny and trophic niches of Rimicaris vent shrimps. *Royal Society Open Science*, *7*(7), 200837. https://doi.org/10.1098/rsos.200837

Methou, P., Nye, V., Copley, J. T., Watanabe, H. K., Nagai, Y., & Chen, C. (2023). Life-history traits of alvinocaridid shrimps inhabiting chemosynthetic ecosystems around Japan. *Marine Biology*, *170*(75), 1–17. https://doi.org/10.1007/s00227-023-04221-4

Methou, P., Ogawa, N. O., Nomaki, H., Ohkouchi, N., Chen, C., & Schnabel, K. (2024). Genetic connectivity and isotopic niches of alvinocaridid shrimps from chemosynthetic habitats in Aotearoa/New Zealand, with a new Alvinocaris species. *Marine Ecology Progress Series*. https://doi.org/10.3354/meps14611

Mitarai, S., Watanabe, H., Nakajima, Y., Shchepetkin, A. F., & McWilliams, J. C. (2016). Quantifying dispersal from hydrothermal vent fields in the western Pacific Ocean. *Proceedings of the National Academy of Sciences of the United States of America*, *113*(11), 2976–2981. https://doi.org/10.1073/pnas.1518395113

Morato, T., Hoyle, S. D., Allain, V., & Nicol, S. J. (2010). Seamounts are hotspots of pelagic biodiversity in the open ocean. *Proceedings of the National Academy of Sciences*, *107*(21), 9707–9711. https://doi.org/10.1073/pnas.0910290107

Pembleton, L. W., Cogan, N. O. I., & Forster, J. W. (2013). St AMPP: An R package for calculation of genetic differentiation and structure of mixed-ploidy level populations. *Molecular Ecology Resources*, *13*(5), 946–952. https://doi.org/10.1111/1755-0998.12129

Pinheiro, H. T., Bernardi, G., Simon, T., Joyeux, J.-C., Macieira, R. M., Gasparini, J. L., Rocha, C., & Rocha, L. A. (2017). Island biogeography of marine organisms. *Nature*, *549*(7670), 82–85. https://doi.org/10.1038/nature23680

Podowski, E. L., Ma, S., Luther, G. W., Wardrop, D., & Fisher, C. R. (2010). Biotic and abiotic factors affecting distributions of megafauna in diffuse flow on andesite and basalt along the Eastern Lau Spreading Center, Tonga. *Marine Ecology Progress Series*, *418*(May), 25–45. https://doi.org/10.3354/meps08797

Poitrimol, C., Thiébaut, E., Daguin-Thiébaut, C., Le Port, A.-S., Ballenghien, M., Tran Lu Y, A., Hourdez, S., & Jollivet, D. (2022). Contrasted phylogeographic patterns of hydrothermal vent

gastropods along South West Pacific: Woodlark Basin, a possible contact zone and/or stepping-stone. *PLoS ONE*, 1–27. https://doi.org/10.1371/journal.pone.0275638

Portik, D. M., Leaché, A. D., Rivera, D., Barej, M. F., Burger, M., Hirschfeld, M., Rödel, M., Blackburn, D. C., & Fujita, M. K. (2017). Evaluating mechanisms of diversification in a Guineo-Congolian tropical forest frog using demographic model selection. *Molecular Ecology*, *26*(19), 5245–5263. https://doi.org/10.1111/mec.14266

Posit team. (2025). *RStudio: Integrated Development Environment for R*. [Computer software]. Posit Software. http://www.posit.co/

Prjibelski, A., Antipov, D., Meleshko, D., Lapidus, A., & Korobeynikov, A. (2020). Using SPAdes De Novo Assembler. *Current Protocols in Bioinformatics*, *70*(e102), 1–29. https://doi.org/10.1002/cpbi.102

Puillandre, N., Brouillet, S., & Achaz, G. (2021). ASAP: Assemble species by automatic partitioning. *Molecular Ecology Resources*, *21*(2), 609–620. https://doi.org/10.1111/1755-0998.13281

R Core Team, . (2021). *R: A language and environment for statistical computing*. Vienna, Austria. https://www.r-project.org

Rambaut, A., Drummond, A. J., Xie, D., Baele, G., & Suchard, M. A. (2018). Posterior Summarization in Bayesian Phylogenetics Using Tracer 1.7. *Systematic Biology*, *67*(5), 901–904. https://doi.org/10.1093/sysbio/syy032

Resing, J. A., Rubin, K. H., Embley, R. W., Lupton, J. E., Baker, E. T., Dziak, R. P., Baumberger, T., Lilley, M. D., Huber, J. A., Shank, T. M., Butterfield, D. A., Clague, D. A., Keller, N. S., Merle, S. G., Buck, N. J., Michael, P. J., Soule, A., Caress, D. W., Walker, S. L., … Thomas, H. (2011). Active submarine eruption of boninite in the northeastern Lau Basin. *Nature Geoscience*, *4*(11), 799–806. https://doi.org/10.1038/ngeo1275

Reynolds, J., Weir, B. S., & Cockerham, C. C. (1983). Estimation of the coancestry coefficient: Basis for a short-term genetic distance. *Genetics*, *105*(3), 767–779. https://doi.org/10.1093/genetics/105.3.767

Ribardière, A., Daguin-Thiébaut, C., Houbin, C., Coudret, J., Broudin, C., Timsit, O., & Broquet, T. (2017). Geographically distinct patterns of reproductive isolation and hybridization in two sympatric species of the *Jaera albifrons* complex (marine isopods). *Ecology and Evolution*, *7*(14), 5352–5365. https://doi.org/10.1002/ece3.3106

Ribardière, A., Pabion, E., Coudret, J., Daguin-Thiébaut, C., Houbin, C., Loisel, S., Henry, S., & Broquet, T. (2021). Sexual isolation with and without ecological isolation in marine isopods *Jaera albifrons* and *J. praehirsuta*. *Journal of Evolutionary Biology*, *34*(1), 33–48. https://doi.org/10.1111/jeb.13559

Rogers, A. D. (2018). The Biology of Seamounts: 25 Years on. In *Advances in Marine Biology* (Vol. 79, pp. 137–224). Elsevier. https://doi.org/10.1016/bs.amb.2018.06.001

Ronquist, F., Teslenko, M., Van Der Mark, P., Ayres, D. L., Darling, A., Höhna, S., Liu, L., Suchard, M. A., & Huelsenbeck, J. P. (2012). MrBayes 3.2: Efficient Bayesian Phylogenetic Inference and Model Choice Across a Large Model Space. *Systematic Biology*, *61*(3), 539–542. https://doi.org/10.1093/sysbio/sys029

Rozas, J., Ferrer-Mata, A., Sanchez-DelBarrio, J. C., Guirao-Rico, S., Librado, P., Ramos-Onsins, S. E., & Sanchez-Gracia, A. (2017). DnaSP 6: DNA sequence polymorphism analysis of large data sets. *Molecular Biology and Evolution*, *34*(12), 3299–3302. https://doi.org/10.1093/molbev/msx248

Santos, H., Rousselet, J., Magnoux, E., Paiva, M.-R., Branco, M., & Kerdelhué, C. (2007). Genetic isolation through time: Allochronic differentiation of a phenologically atypical population of the pine processionary moth. *Proceedings of the Royal Society B: Biological Sciences*, *274*(1612), 935–941. https://doi.org/10.1098/rspb.2006.3767

Schnur, S. R., Chadwick, W. W., Embley, R. W., Ferrini, V. L., De Ronde, C. E. J., Cashman, K. V., Deardorff, N. D., Merle, S. G., Dziak, R. P., Haxel, J. H., & Matsumoto, H. (2017). A decade of volcanic construction and destruction at the summit of NW Rota-1 seamount: 2004–2014. *Journal of Geophysical Research: Solid Earth*, *122*(3), 1558–1584.

https://doi.org/10.1002/2016JB013742

Skotte, L., Korneliussen, T. S., & Albrechtsen, A. (2013). Estimating Individual Admixture Proportions from Next Generation Sequencing Data. *Genetics*, *195*(3), 693–702. https://doi.org/10.1534/genetics.113.154138

Stankowski, S., Westram, A. M., Zagrodzka, Z. B., Eyres, I., Broquet, T., Johannesson, K., & Butlin, R. K. (2020). The evolution of strong reproductive isolation between sympatric intertidal snails. *Philosophical Transactions of the Royal Society B: Biological Sciences*, *375*(1806), 20190545. https://doi.org/10.1098/rstb.2019.0545

Stern, R. J., Fouch, M. J., & Klemperer, S. L. (2003). An overview of the Izu-Bonin-Mariana subduction factory. In J. Eiler (Ed.), *Geophysical Monograph Series* (Vol. 138, pp. 175–222). American Geophysical Union. https://doi.org/10.1029/138GM10

Stothard, P., & Wishart, D. S. (2004). Circular genome visualization and exploration using CGView. *Bioinformatics*, *21*(4), 537–539. https://doi.org/10.1093/bioinformatics/bti054

Székely, T., Weissing, F. J., & Komdeur, J. (2014). Adult sex ratio variation: Implications for breeding system evolution. *Journal of Evolutionary Biology*, *27*(8), 1500–1512. https://doi.org/10.1111/jeb.12415

Tajima, F. (1983). Evolutionary relationship of DNA sequences in finite populations. *Genetics*, *105*(2), 437–460. https://doi.org/10.1093/genetics/105.2.437

Teixeira, S., Serrão, E. A., & Arnaud-Haond, S. (2012). Panmixia in a fragmented and unstable environment: The hydrothermal shrimp Rimicaris exoculata disperses extensively along the Mid-Atlantic ridge. *PLoS ONE*, *7*(6), 1–10. https://doi.org/10.1371/journal.pone.0038521

Thaler, A. D., Plouviez, S., Saleu, W., Alei, F., Jacobson, A., Boyle, E. A., Schultz, T. F., Carlsson, J., & Van Dover, C. L. (2014). Comparative population structure of two deep-sea hydrothermal-vent-associated decapods (Chorocaris sp. 2 and Munidopsis lauensis) from southwestern Pacific back-arc basins. *PLoS ONE*, *9*(7), 1–13. https://doi.org/10.1371/journal.pone.0101345

Thomas-Bulle, C., Bertrand, D., Nagarajan, N., Copley, R. R., Corre, E., Hourdez, S., Bonnivard, É.,

Claridge-Chang, A., & Jollivet, D. (2022). Genomic patterns of divergence in the early and late steps of speciation of the deep-sea vent thermophilic worms of the genus Alvinella. *BMC Ecology and Evolution*, *22*(1), 106. https://doi.org/10.1186/s12862-022-02057-y

Tran Lu Y, A., Ruault, S., Daguin-Thiébaut, C., Castel, J., Bierne, N., Broquet, T., Wincker, P., Perdereau, A., Arnaud-Haond, S., Gagnaire, P.-A., Jollivet, D., Hourdez, S., & Bonhomme, F. (2022). Subtle limits to connectivity revealed by outlier loci within two divergent metapopulations of the deep-sea hydrothermal gastropod Ifremeria nautilei. *Molecular Ecology*, 1–46. https://doi.org/10.1111/mec.16430

Tran Lu Y, A., Ruault, S., Daguin-Thiébaut, C., Le Port, A.-S., Ballenghien, M., Castel, J., Gagnaire, P.-A., Bierne, N., Arnaud-Haond, S., Poitrimol, C., Thiebaut, E., Lallier, F., Broquet, T., Jollivet, D., Bonhomme, F., & Hourdez, S. (2025). Comparative Population Genomics Unveils Congruent Secondary Suture Zone in Southwest Pacific Hydrothermal Vents. *Molecular Biology and Evolution*, *42*, 1–16. https://doi.org/10.1093/molbev/msaf024

Tunnicliffe, V., Chen, C., Giguère, T., Rowden, A. A., Watanabe, H. K., & Brunner, O. (2023). Hydrothermal vent fauna of the western Pacific Ocean: Distribution patterns and biogeographic networks. *Diversity and Distributions*, ddi.13794. https://doi.org/10.1111/ddi.13794

Tunnicliffe, V., McArthur, A. G., & McHugh, D. (1998). A Biogeographical Perspective of the Deep-sea Hydrothermal Vent Fauna. *Advances in Marine Biology*, *34*. https://doi.org/10.1016/S0065-2881(08)60213-8

Vieira, F. G., Lassalle, F., Korneliussen, T. S., & Fumagalli, M. (2016). Improving the estimation of genetic distances from Next-Generation Sequencing data. *Biological Journal of the Linnean Society*, *117*(1), 139–149. https://doi.org/10.1111/bij.12511

Waples, R. S., & Gaggiotti, O. (2006). What is a population? An empirical evaluation of some genetic methods for identifying the number of gene pools and their degree of connectivity. *Molecular Ecology*, *15*(6), 1419–1439. https://doi.org/10.1111/j.1365-294X.2006.02890.x

Weigelt, P., Steinbauer, M. J., Cabral, J. S., & Kreft, H. (2016). Late Quaternary climate change shapes island biodiversity. *Nature*, *532*(7597), 99–102. https://doi.org/10.1038/nature17443

Whittaker, R. J., Triantis, K. A., & Ladle, R. J. (2008). A general dynamic theory of oceanic island biogeography. *Journal of Biogeography*, *35*(6), 977–994. https://doi.org/10.1111/j.1365-2699.2008.01892.x

Wickham, H., Averick, M., Bryan, J., Chang, W., McGowan, L., François, R., Grolemund, G., Hayes, A., Henry, L., Hester, J., Kuhn, M., Pedersen, T., Miller, E., Bache, S., Müller, K., Ooms, J., Robinson, D., Seidel, D., Spinu, V., … Yutani, H. (2019). Welcome to the Tidyverse. *Journal of Open Source Software*, *4*(43), 1686. https://doi.org/10.21105/joss.01686

Williams, A. B., & Dobbs, F. C. (1995). A new genus and species of caridean shrimp (Crustacea: Decapoda: Bresiliidae) from hydrothermal vents on Loihi Seamount, Hawaii. *Proceedings of the Biological Society of Washington*, *108*(2), 228–237.

Yahagi, T., Watanabe, H., Ishibashi, J. I., & Kojima, S. (2015). Genetic population structure of four hydrothermal vent shrimp species (Alvinocarididae) in the Okinawa Trough, Northwest Pacific. *Marine Ecology Progress Series*, *529*, 159–169. https://doi.org/10.3354/meps11267

Zhou, Y., Chen, C., Zhang, D., Wang, Y., Kayama, H., Jin, W., Dass, S., Ruiyan, B., Han, Y., Sun, D., Xu, P., Lu, B., Zhai, H., Han, X., Tao, C., Qiu, Z., Sun, Y., Liu, Z., Qiu, W., & Wang, C. (2022). Delineating biogeographic regions in Indian Ocean deep-sea vents and implications for conservation. *Diversity and Distributions*, *April*, 1–13. https://doi.org/10.1111/ddi.13535

Data Accessibility & Benefit-Sharing

Data Accessibility

All *COI* barcode sequences have been deposited in GenBank under accession numbers DQ328819 – DQ328837 and PQ643496 – PQ643653 (see Table S10 for details on haplotype numbers and localities with associated individual ID). Raw sequences of the WGS sequencing dataset are available in the NCBI SRA repository with the BioProject ID PRJNA1197504 (Accession numbers: SAMN45807939 – SAMN45807966). Details information on sampling localities, sampling date, sex,

life stages and sizes of individuals analysed for population sex ratio and reproduction are compiled in a table sheet named “Population_dataset” in supplementary material.

Benefit-sharing

Faunal collections were conducted with the necessary authority permissions of the relevant countries. Sampling in the Japanese exclusive economic zone (EEZ) and the Mariana EEZ were respectively conducted by Japanese government and American government research vessels. Permission for sampling in the Tongan EEZ was issued by the Kingdom of Tonga. Research animals were invertebrate caridean shrimps and no live experiments with animals were conducted in this study.

Figure Captions

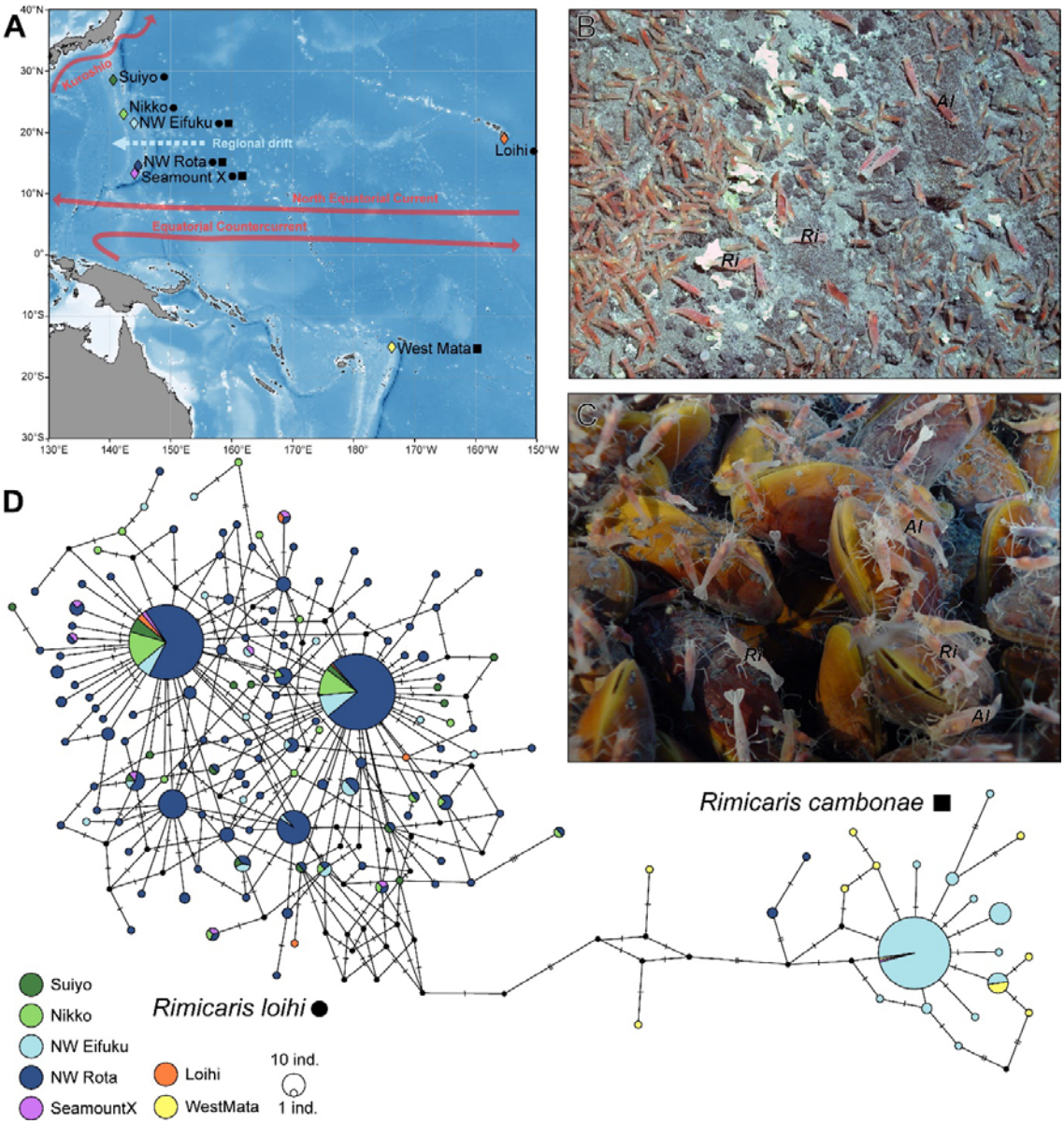

Figure 1. A. Geographic distribution of samples for *Rimicaris cambonae* (square) and *Rimicaris loihi* (circle). Coloured diamonds indicates localities and black shapes (circles and squares) indicates species. Typical habitats of *Rimicaris spp.* (*Ri*) on (**B**) sulfur crusts (NW Rota, 2009) and (**C**) mussel beds (NW Eifuku, March 2004). **D.** *COI* haplotype network (529 bp) of *Rimicaris* species from Loihi, West Mata and the Mariana Arc vent fields (n= 597) detailed per sampling site. Two clusters emerge with 24 haplotypes affiliated with *R. cambonae* and 134 haplotypes affiliated with *R. loihi*.

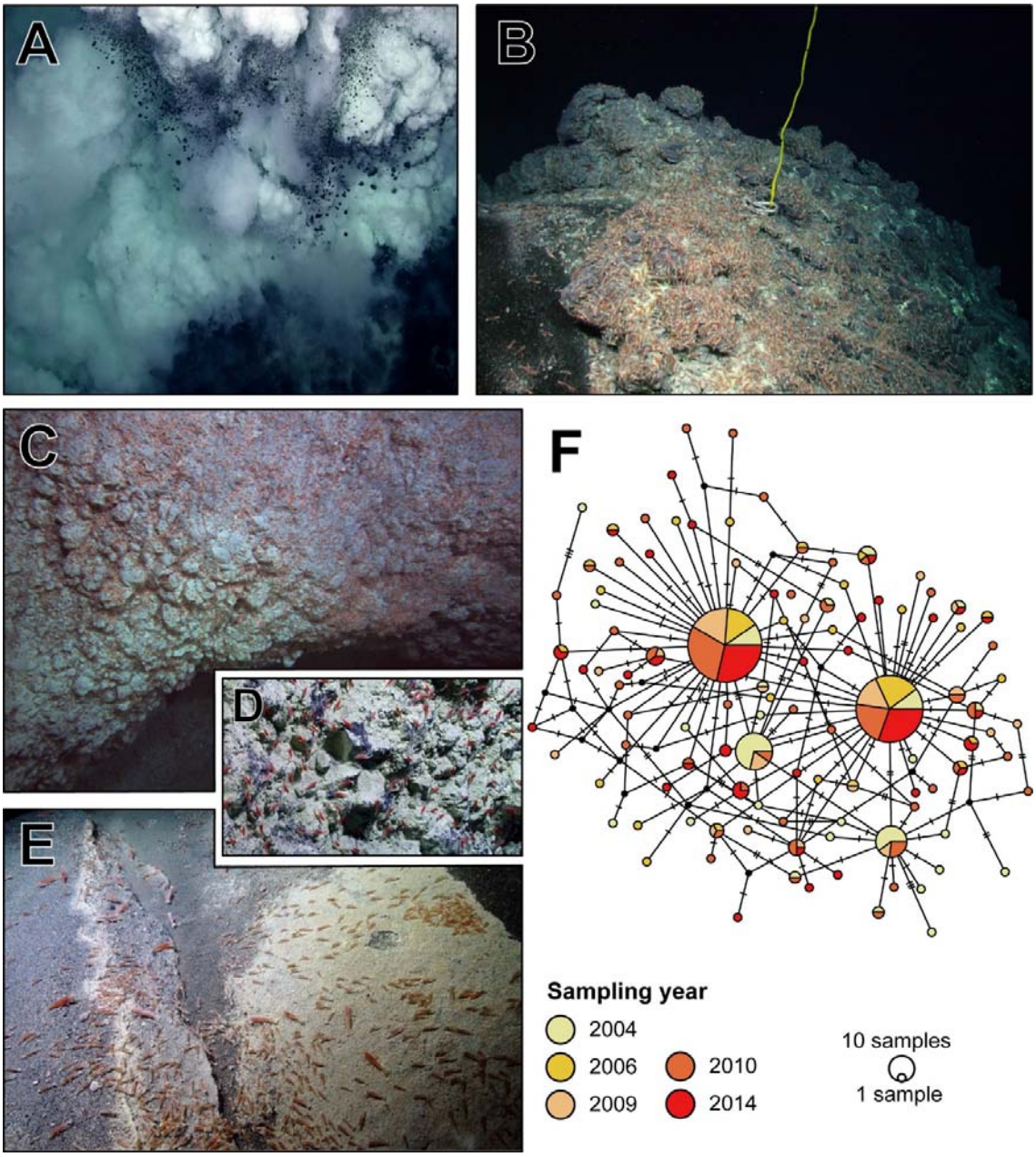

Figure 2. Temporal metapopulation dynamics of *Rimicaris loihi* at NW Rota between 2004 and 2014. **A.** Eruptive pit with explosive ejection of tephra and sulphur at Brimstone Pit in April 2006. **B.** Abundant shrimps near Marker 109 in April 2009. **C.** New shrimp recruits on sulphur wall in March 2010; red laser dots in the center of image are 10 cm apart. **D.** Close up view of small shrimp recruits on sulphur wall**. E**. Shrimp in lower abundance in December 2014. **F.** *COI* haplotype network of *Rimicaris loihi* from NW Rota (n= 332) detailed per sampling year.

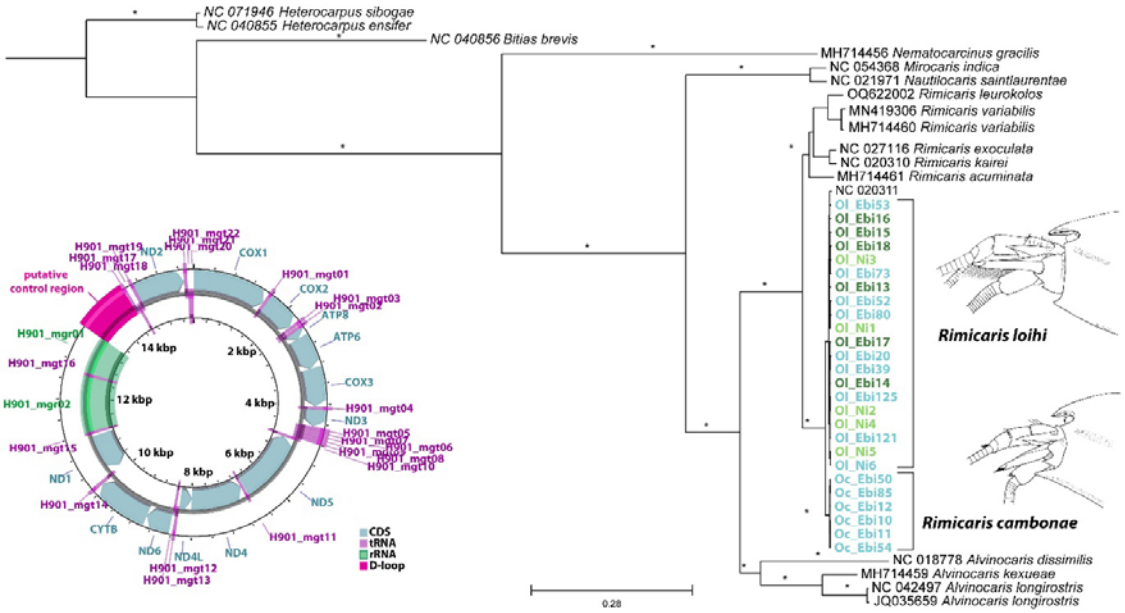

911

912 **Figure 3.** Bayesian estimation of phylogeny of mitochondrial genomic data for Alvinocaridae
913 including *R. loihi* and *R. cambonae* samples from Suiyo, Nikko, and NW Eifuku seamounts with the
914 GTR+I+Γ model for 17,813 sites and a representation of the gene position, type, and order in the
915 mitogenome of *R. loihi* and *R. cambonae.* * indicates 1.0 posterior probability.

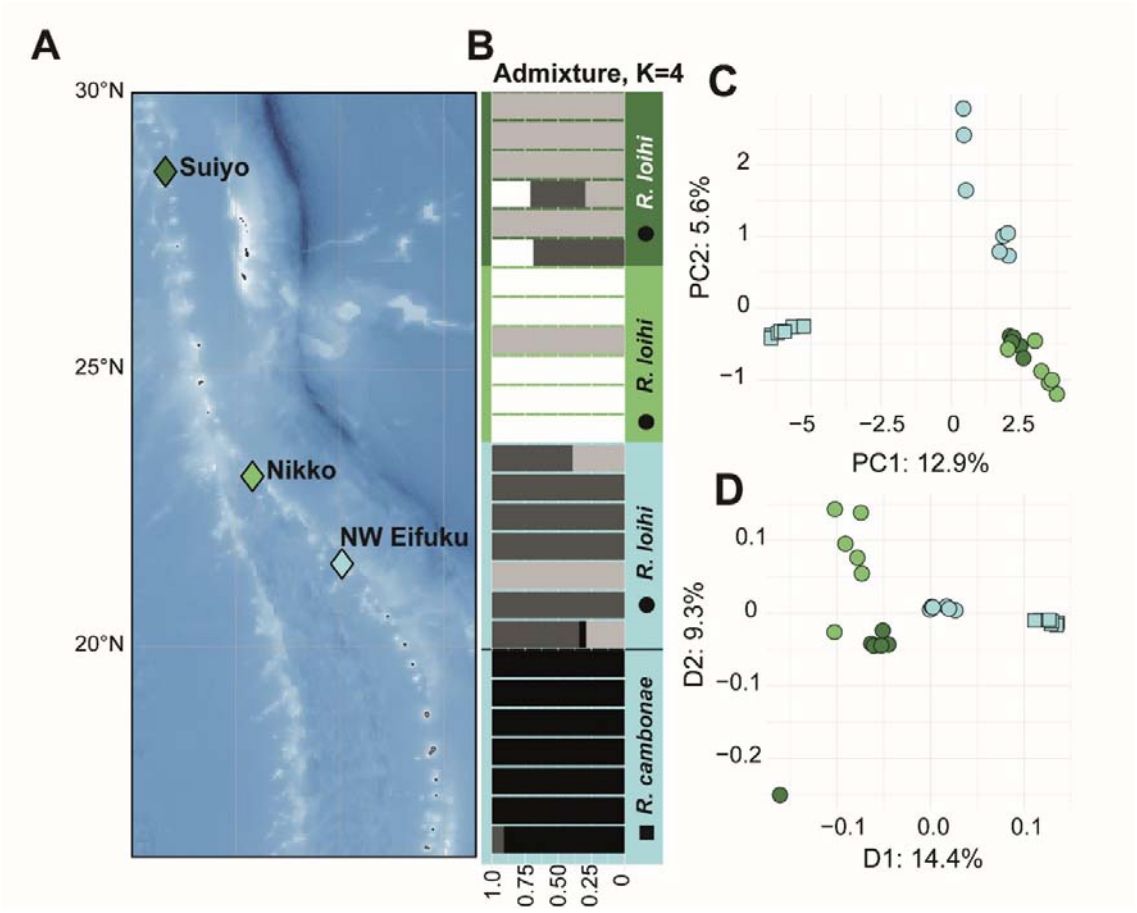

Figure 4. A. Map of sampling localities included in population genomic analyses for *R. cambonae* and *R. loihi* including Suiyo Seamount (dark green), Nikko Seamount (light green) and NW Eifuku Seamount (blue) including dominant current vectors from Mitarai et al 2016 (arrows). **B.** Admixture plot for four populations (K=4) including 26 individuals for 111002 loci. **C.** Plot of first two axes of principal component analyses (PCA) for 111002 loci. **D.** Plot of first two dimensions for multiple dimensional scaling (MDS) estimates from 126652 loci based on genetic distances for *R. cambonae* (squares) and *R. loihi* (circles).

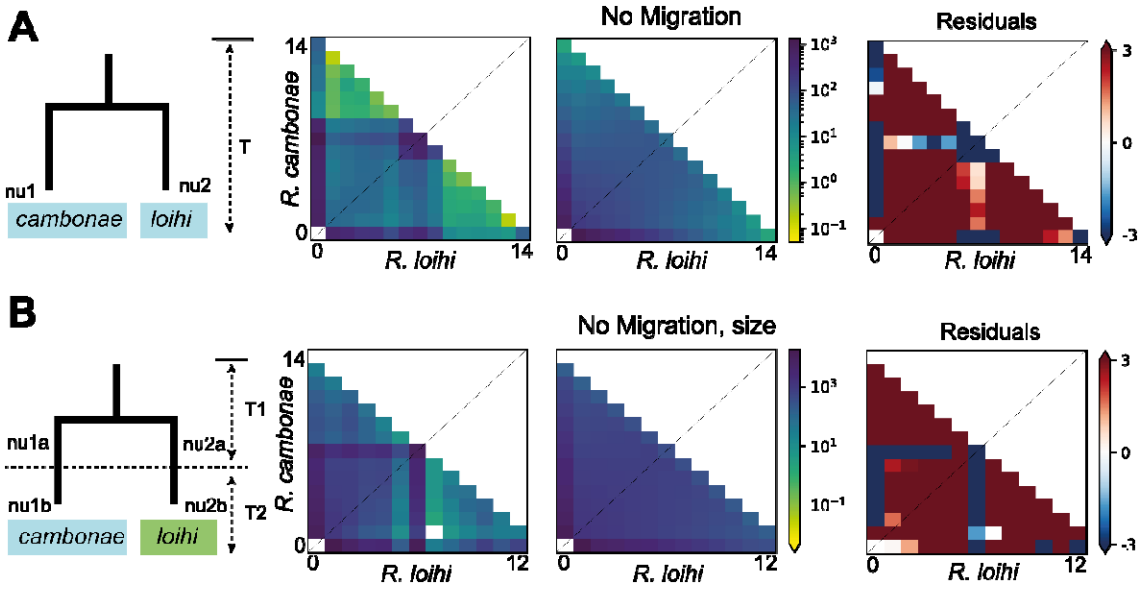

Figure 5. Graphics for the most likely models for dadi_pipeline results and the joint folded allele frequency spectra (AFS), fitted AFS and residuals for **A.** Sympatry: No migration between sympatric populations of seven *R. cambonae* and seven *R. loihi* from Eifuku Seamount and **B.** Allopatry: No migration with population size change between allopatric populations of seven *R. cambonae* and six *R. loihi* from Nikko Seamount. Cell darkness corresponds to the number of minor alleles in the given bin for both *R. loihi* and *R. cambonae*.

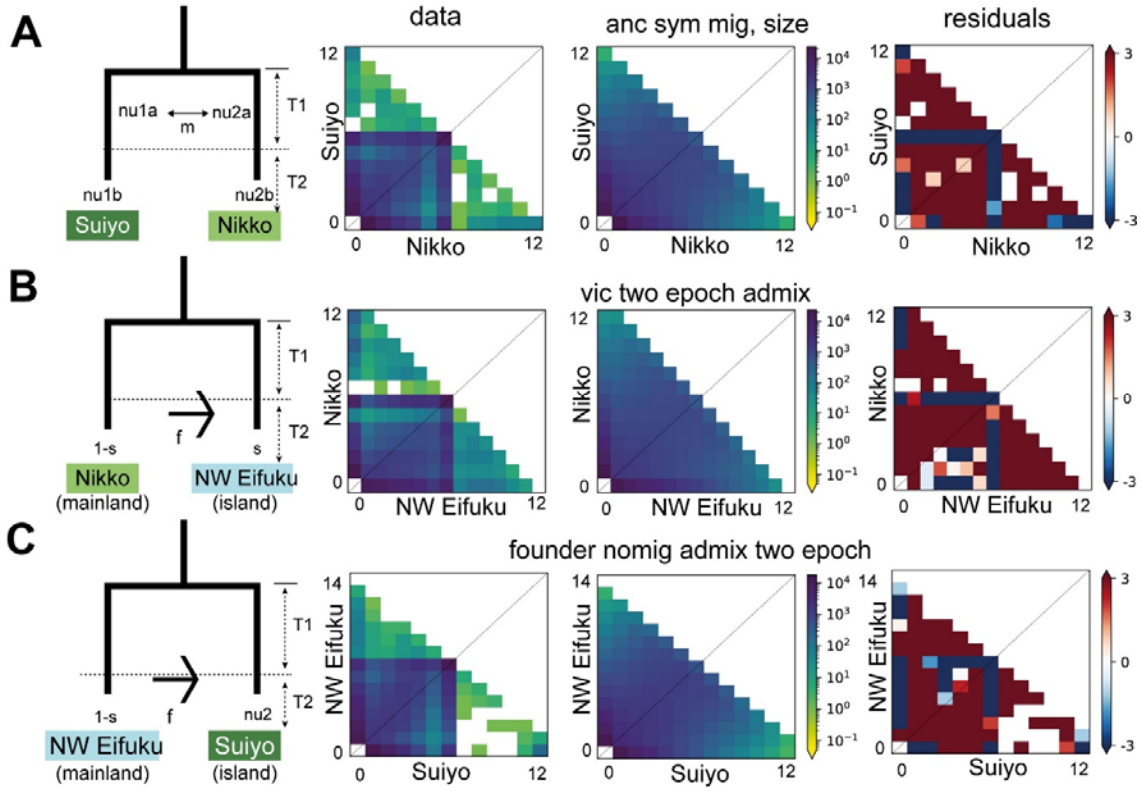

Figure 6. Graphics of the most likely models from dadi_pipeline results and the joint folded allele frequency spectra (AFS), fitted AFS, and residuals within *R. loihi* for **A.** Ancestral symmetrical migration with size changes between Suiyo and Nikko Seamount, **B.** Island model of vicariance, middle unidirectional discrete admixture event between two drift events between Nikko and NW Eifuku Seamount and **C.** The island model for a founder event with a middle unidirectional discrete admixture event between two drift events for Eifuku and Suiyo seamount. Cell darkness corresponds to the number of minor alleles in the given bin for both populations.

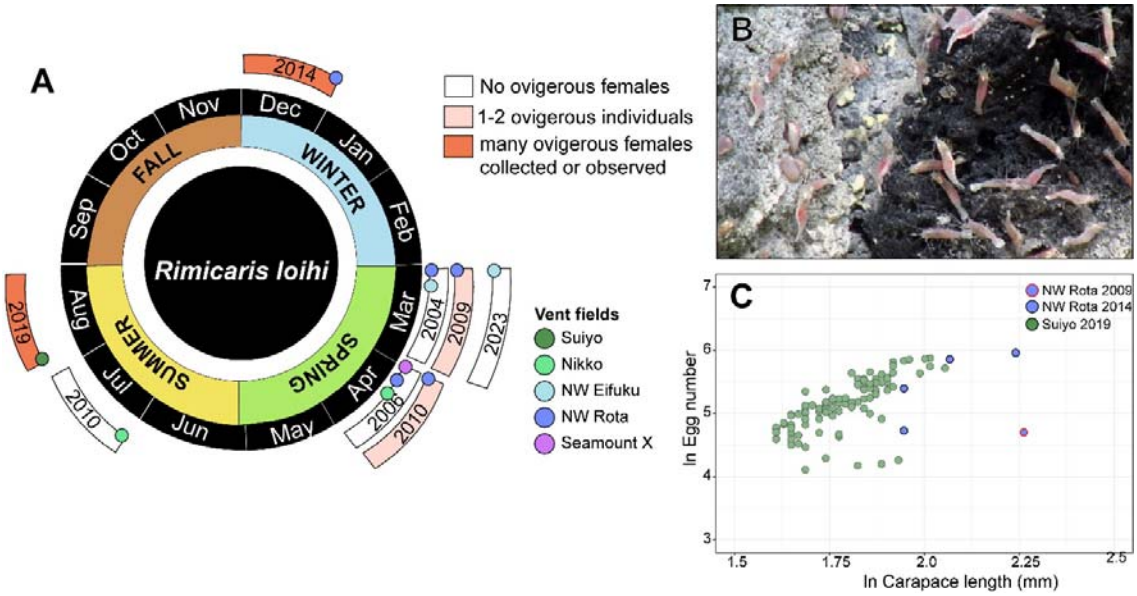

Figure 7. Reproductive characteristics of *Rimicaris loihi*. **A.** Diagrams summarizing the occurrence of *R. loihi* ovigerous females over sampling realized between 2004 and 2019. **B.** Numerous ovigerous females (reddish colour below the abdomen) observed, but not collected, at NW Rota in December 2014. **C.** Relative fecundity of *R. loihi* displayed by $\log_e$-transformed number of eggs with $\log_e$-transformed carapace length (CL). Data from Suiyo are from Methou et al. (2023). Data from NW Rota are from this study.

Vent field	Year	Species	M	F	M:F	χ^2	*p*
NW Rota	2009	*Rimicaris loihi*	119	211	0.56	25.65	***
NW Rota	2010	*Rimicaris loihi*	395	797	0.49	135.57	***
NW Rota	2014	*Rimicaris loihi*	47	380	0.12	259.69	***
Suiyo[(1)]	2019	*Rimicaris loihi*	145	235	0.62	22.94	***
NW Eifuku	2023	*Rimicaris loihi*	4	8	0.5	1.33	NS
NW Eifuku	2023	*Rimicaris cambonae*	60	72	0.83	1.09	NS

Table 1. Population characteristics with sex ratio of *Rimicaris cambonae* and *Rimicaris loihi* from NW Rota, Suiyo and NW Eifuku. [(1)] Data from Suiyo are from Methou et al. (2023). M: males, F: females; Significance levels: NS: > 0.05, *: < 0.05, **: < 0.01, ***: < 0.00.

Year	Volcanic state	Hydrothermal State	Shrimp population
2004	Volcanic vent in a deep pit with surging sulphurous plume and ejecta; mass wasting on volcano flank.[(1)]	13 discrete low temperature vents and seeping around rim of volcanic pit.	Extensive: dense at vents and scattered across summit; 37%
2006	Explosive eruptions from pit observed after sidewall collapse; ejecta volume to 100 m^3/hr.[(2)]	Discrete sites fewer; seeping through sediments near pit; eastern scarp more focussed.	Restricted: scattered near pit; concentrated at three sites; 12%.
2009	Up to 47 m of tephra accumulated since 2004[(3)]; ejecta evident.	Many discrete venting sites <50°C broadly distributed across summit; venting through sediments.	Very extensive: dense at vents and scattered across summit; 45%
2010	Recent eruption reshaped the summit[(3)]; now several volcanic orifices	Loss of several vents in landslide; exposed walls covered with sulphur;	Very extensive: dense at vents; scattered on summit and on new exposed walls; 40%.
2014	No eruptive activity[(4)]; likely quiescence >1 year.	No or negligible activity at all former sites; only notable temperature anomaly around pit.	Restricted mostly to one site; other locations limited or abandoned; 6%.

Table 2. History of observed volcanism and venting on NW Rota. The relative extent of the shrimp populations is assessed by estimating the % of ROV tracks in which shrimp were greater than 20 individuals/m^2. [(1)]Embley et al. 2006; [(2)]Chadwick et al. 2008; [(3)]Chadwick et al. 2012; [(4)]Schnur et al. 2014.